CuO/TiO_2 nanocomposite photocatalyst for efficient MO degradation

A. I. M. A'srai[a], M. H. Razali[a,b], K. A. M. Amin[a,b], U. M. Osman[a,b*]
[a]*Faculty of Science and Marine Environment, Universiti Malaysia Terengganu 21030, Kuala Nerus, Terengganu, Malaysia*
[b]*Advanced Nanomaterials Research Group, Faculty of Science and Marine Environment, Universiti Malaysia Terengganu, 21030 Kuala Nerus, Terengganu, Malaysia*

Many studies have been performed to degrade the methyl orange (MO) dye by introducing titanium dioxide (TiO_2) semiconductor material as photocatalyst because TiO_2 having unique characterizations such as low toxicity and good chemical stability. However, its photocatalytic reaction is limited by low surface area as well as the rapid recombination of photogenerated electron-hole pairs and only has ability to absorb a small fraction (<5%) of indoor light. Therefore, in this study, copper oxide/titanium dioxide (CuO/TiO_2) nanocomposite photocatalyst was proposed and synthesized using wet precipitation method. The synthesised photocatalyst was characterized by using Fourier-transform infrared spectroscopy (FTIR), X-ray diffraction analysis (XRD), Scanning electron microscopy (SEM), Energy dispersive x-ray (EDX), Thermogravimetric analysis (TGA), Nitrogen gas adsorption-desorption Brunauer, Emmett, teller (BET) and UV-Visible Spectroscopy. Spectra obtained from FTIR have proved that there are existence of O-H stretching, O-H bending and metal-oxygen bond that correlates to the functional groups of the samples. As affirmed by XRD analysis, crystalline anatase TiO_2 phase was obtained for pure TiO_2 samples. Anatase TiO_2 phase is remained, and the additional peaks belong to copper oxide was observed for CuO/TiO_2 nanocomposite photocatalyst sample suggesting that copper oxide was successfully loaded onto TiO_2. The morphological study from SEM shows the presence of irregular particles of copper oxide and agglomerated TiO_2 bulk particles. The CuO/TiO_2 nanocomposite photocatalyst's presence of copper, titanium, and oxygen was confirmed by EDX analysis. TGA results show that pure CuO, TiO_2 and CuO/TiO_2 nanocomposite photocatalyst were thermally stable as only 6.7, 6.8 and 7.9 % weight loss were observed, due to the water removal. The specific surface area of CuO, TiO_2 and CuO/TiO_2 composite photocatalysts were found to be 20.50 m^2/g, 15.26 m^2/g and 37.12 m^2/g, respectively. They also exhibit type IV isotherms which is indicated the presence of mesopores in sample. This mesoporous structure provided high pore size within 2 to 50 nm in the sample. The photocatalytic activity study demonstrates that the 1.0 g CuO/TiO_2 with the ratio of (0.5:1) could degraded 90.46 % of 10 ppm Methyl Orange (MO) dye at pH 6, which is better than pure TiO_2, pure CuO and other CuO/TiO_2 nanocomposites after 3 hours reaction. This is attributed to the presence of CuO at optimum amount which can increased the surface area, promoted electron-hole separation, and decelerated the charge carrier recombination. At 1 ppm MO, 100 % degradation was observed using similar photocatalyst and condition. However, the degradation rate of Methylene Blue (MB) and phenol was slightly reduced to almost 95.47 % and 80.65 % after 180 minutes reaction, due to their chemical structure and stability.

(Received March 25, 2023; Accepted September 11, 2023)

Keywords: Copper oxide, Degradation, Nanocomposite, Photocatalyst, Titanium dioxide

1. Introduction

Textiles industry is one of the most dirtying enterprises in wording of the volume and the many-sided quality of treatment of their effluents release. It has been accounted for that wastewater produced by textile industries are known to contain generous measures of harmful

* Corresponding author: uwais@umt.edu.my
https://doi.org/10.15251/DJNB.2023.183.1105

aromatic mixes, particularly azo dyes such as MO [1]. Therefore, many studies have been performed to remove the MO dye by introducing titanium dioxide (TiO_2) semiconductor material that has property only active in the ultraviolet (UV) light range, and the quantum yield is not satisfying [2]. Titanium dioxide (TiO_2) having unique characterizations such as high photocatalytic activity, low toxicity, and good chemical stability is extensively used as photocatalyst [3]. Nevertheless, poor photocatalytic performance of TiO_2 in the visible region, owing to the wide band gap (3.2 eV), has been limited its application [4]. Therefore, some efforts have been taken to overcome the problem and improve the photocatalytic activity of TiO_2, including doping [5], surface modification [6] or combination of semiconductor oxides [7]. These modifications can generate electron-hole by the irradiation of visible light and expand their separation period, resulting in a greater photocatalytic activity [8]. Among metal oxides, copper oxide (CuO), with band gap energy of 2.1 ev [9], have attracted significant attention for semiconductor combination, due to low cost, non-toxicity, good optical and catalytical properties, as well as superior activity in the visible region [10,11]. There are important studies that report on photocatalysis recently. For example, Gupta *et al.* reported high decolorization rate and efficiency of azo dyes by the combination of TiO_2 and UV [12,13] for environment purification to treat contamination in the water. Mingmongkol confirmed that the combination of TiO_2 and CuO metal oxides can change the recombination rate of photogenerated electrons and holes, and effectively obtain higher photocatalytic activity [14]. CuO is a kind of p-type semiconductor material with a narrow bandgap. The coupling of CuO semiconductor with TiO_2 semiconductor forms p-n heterojunction photocatalyst, which inhibits the recombination rate of photogenerated electron pairs to the enhancement of the charge separation, improves the light capture ability irradiation absorption of the catalyst and enhances the photocatalytic activity [15,16]. So, in this study, copper oxide with titanium dioxide nanocomposite photocatalyst have been synthesized, characterized and tested for methyl orange dye degradation.

2. Materials and methods

2.1. Materials

All the chemicals and components required to create the copper oxide/titanium dioxide (CuO/TiO_2) nanocomposite photocatalyst were bought commercially from authorized manufacturers. Without additional purification, all chemicals and solvents were use as obtained. As a precursor to TiO_2, commercial titanium dioxide powder from Merck (Germany) was used. Distilled water was used to dilute sodium hydroxide (NaOH) pellets from Merck (Germany) to create 10 M NaOH aqueous solutions. To create 0.1 M HCl aqueous solution, hydrochloric acid (HCl, 37 % solution in water), also purchased from Merck (Germany), was diluted with distilled water. Methyl orange (MO), copper sulphate pentahydrate ($CuSO_4.5H_2O$) and deionized water.

2.2. Synthesis of CuO/TiO_2 nanocomposite photocatalyst

Under magnetic stirring, 400 ml of deionized water was used to dissolve 0.5 g of $CuSO_4.5H_2O$. The solution was then given 1.0 g of TiO_2 and stir for 3 hours to create a uniform suspension. The pH of the solutions was then brought to 11 by adding NaOH to the suspension. Flocky precipitate then started to develop in the cloudy solution. The solution was then heated at 90 °C for 12 hours, resulting in a grey precipitate at the bottom of the solution as it turned from cloudy to colourless. The precipitate was separated by filtration after being repeatedly washed with deionized water and ethanol, and it was then dried in an oven for 24 hours at 80 °C. The recovered product was then calcined in a furnace for five hours at 400 °C. Similar techniques were utilised to create CuO/TiO_2 nanocomposite photocatalysts with various weight ratios that are (0.25:1, 0.5:1, 1:1, 3:1, 5:1, 8:1).

2.3. Photocatalytic performance test

A photocatalytic degradation experiment was conducted in a beaker that was enclosed in a compartment to block out light in order to determine the photocatalyst's photocatalytic performance. A UV lamp with a 6 W output and a maximum intensity of 354 nm is mounted on

top as a source of UV radiation. Typically, 100 ml of MO (20 ppm) solution was added to 0.1 g of TiO_2 photocatalyst powder, and for 30 minutes, the suspension was stirred in the dark to achieve the adsorption-desorption equilibrium. Following that, 10 ml of the solution is removed, filtered using a 0.45 µm filter membrane, and then recorded as a sample in a darkened space. A further 150 minutes of the photocatalytic degradation reaction were subsequently conducted while being exposed to UV light. The absorption spectra were measured using a UV vis-spectrophotometer, and the percentage of methylene blue degradation was estimated using Eq.(1).

$$\% \, degradation = \frac{C_o - C_t}{C_o} \times 100 \quad (1)$$

where;
C_o is the initial absorption spectra of the dye
C_t is the absorption spectra of dye after reaction at *t* time

3. Results and discussion

3.1. FTIR spectroscopy

The bonding interactions and functional groups of the photocatalyst were studied using FTIR spectroscopy. Figure 1 shows the FTIR spectra of CuO, TiO_2, and CuO/TiO_2 (1:1) nanocomposite photocatalyst samples. A wide peak between 3500 and 3400 cm^{-1} were observed in Figure 1(a) and (b), were assigned to O-H stretching mode of H_2O indicating that the Water molecules (H_2O) were found on the surface of pure CuO and TiO_2. Another peak assinged to O-H bending from water molecules can be observed at ~1600 cm^{-1} in the spectra of pure CuO and TiO_2 samples. While, CuO/TiO_2 (1:1) nanocomposite photocatalyst sample free of water molecules and other contaminants because just one broad band with the highest intensity was seen below 1000 cm-1. at 663.51 cm^{-1} in Figure 1(c) due to the metal and oxygen (M-O) bond. A strong absorption band at 663.51 cm^{-1} shows the presence of both Ti–O and Cu–O in the sample as well as the chemical interaction among them. The M-O bond also appeared in the pure CuO and TiO_2 samples with low intesity attributed to the single Cu-O and Ti-O bonds, respectively.

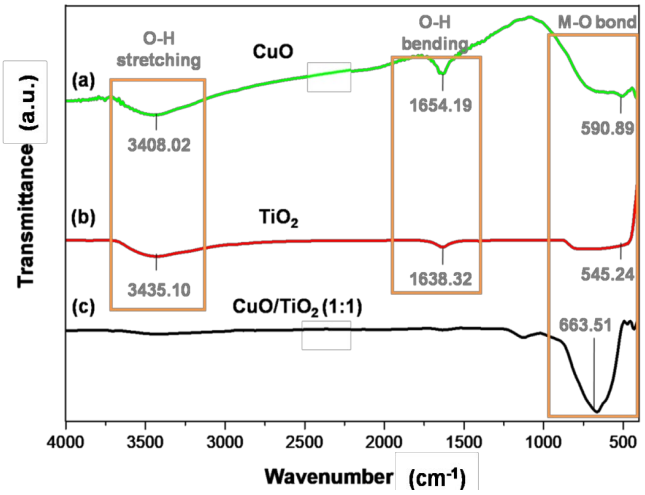

Fig. 1. FTIR spectra of photocatalyst (a) CuO, (b) TiO_2 and (c) CuO/TiO_2 (1:1).

The FTIR spectra of CuO/TiO_2 at different ratio are illustrated in Figure 2. The peak between 1000 and 400 cm^1 is due to Cu-O and Ti-O symmetric stretching of the metal and oxygen. The intensity of the peak is reduced in nanocomposite photocatalyst when the concentration of CuO was increased indicating the presence of chemical interaction from CuO and TiO_2 (Reddy *et*

al., 202). Thus, it was confirmed that the CuO/TiO_2 is successfully synthesized in this research.

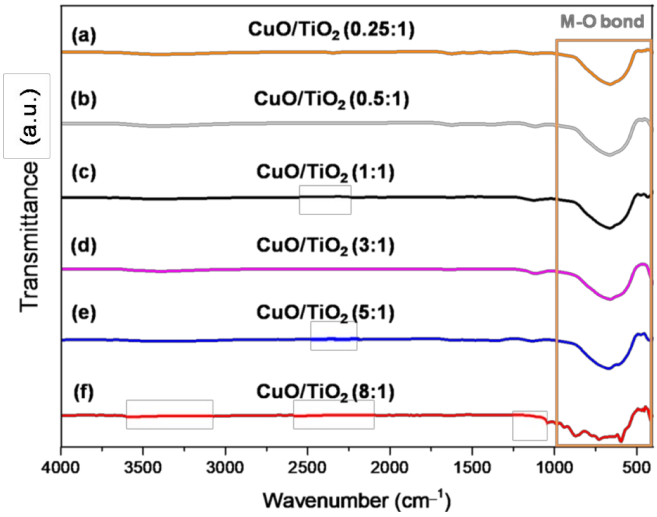

Fig. 2. FTIR spectra of CuO/TiO_2 nanocomposite photocatalyst at various ratio (0.25:1), (0.5:1), (1:1), (3:1), (5:1) and (8:1).

3.2. X-ray diffraction

Copper oxide (CuO), titanium dioxide (TiO_2), and copper oxide/titanium dioxide (CuO/TiO_2) nanocomposite photocatalyst's characteristic XRD patterns were represented in Figure 3. All samples showed a very defined, sharp, and narrow peak, indicating the production of a highly crystalline sample. As shown in Figure 1.3(a), for CuO sample a sharp peak were seen with great intensity at 2 thetas of 32.17°, 35.56°, 38.68°, 48.81°, 56.45°, 58.29°, 61.54°, 66.21°, 68.03° and 75.27° which are assigned to (110), (002), (111), (20-2), (021), (202), (11-3), (022), (113) and (004) of monoclinic CuO. According to the data obtained, the peaks displayed were indicative of copper oxide's chemical composition as reported from another researcher (Tsai *et* al., 2018). Additionally, there were two peaks at 31.74° and 45.49° with the highest intensities, which were attributed to the (110) Cu_2O and (111) Cu, respectively. This result indicates that the sample contains Cu^{2+} (CuO), Cu^{+}, and Cu^{0}.

Figure 3(b) displays the XRD pattern of pure TiO_2 with peaks at 25.3°, 37.8°, 48.0°, 53.9°, 55.1°, 62.7°, 68.8°, 70.3°, and 75.0° that can be indexed to (101), (004), (200), (105), (211), (204), (116), (220), and (215) tetragonal crystal planes of anatase TiO_2 (Liu *et al.,* 2014). For CuO/TiO_2 (1:1) nanocomposite photocatalyst sample one peak belong to anatase TiO_2 (101) was observed at 25.33°. In addition, two peaks assigned to monoclinic CuO (002) and (111) planes 35.48°, and 38.73° and respectively suggesting that only Cu^{2+} species present in this sample.

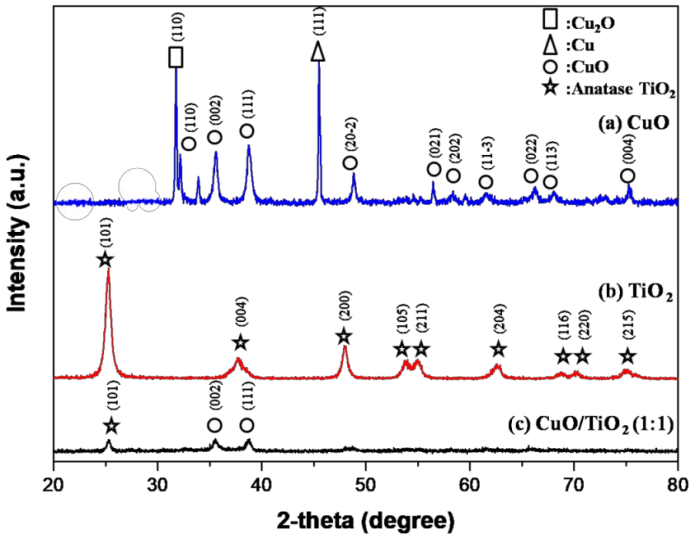

Fig. 3. XRD pattern of (a) CuO, (b) TiO_2 and (c) CuO/TiO_2 (1:1).

This result shows that the Cu species in the CuO/TiO_2 nanocomposite (1:1) sample was fully oxidized into Cu^{2+}(CuO) since Cu^{2+} is a the most stable state. As compared to pristine CuO sample various Cu species was obtained such as Cu, Cu+ and Cu^{2+}. For further investigation to determine how concentrations of CuO affect the XRD analysis of CuO/TiO_2 at different ratio was carried out in Figure 4.

As shown in Figure 4, it is obvious that the CuO/TiO_2 nanocomposite photocatalyst with different ratio of CuO exhibited a different XRD patterns. The nanocomposite photocatalyst samples' XRD patterns can be attributed to the standard of tetragonal anatase TiO_2, rutile TiO_2, and monoclinic CuO (Liu *et al.,* 2014; Reddy *et al.,* 2020; Tsai *et al.,* 2018). No formation of new compound either secondary or tertiary compounds, even after the addition of CuO into TiO_2 up to (8:1) weight ratio.

Peaks at 2θ of 25.32°, 37.95°, 48.04°, 54.09°, 55.11°, and 62.56° were found for the CuO/TiO_2 (0.25:1) nanocomposite photocatalyst sample and might be attributed to the (101), (004), (200), (105), (211), and (204) crystal planes of anatase TiO_2. Similar XRD pattern of CuO/TiO_2 (0.5:1) sample with (0.25:1) ratio was observed suggesting that the addition of CuO up to 0.5 weight ratio could not change the crystal structure of the sample. In addition, no peaks belong to CuO was appeared because small amount of CuO used in these samples. However, we did not clearly observe the XRD peaks corresponding to the CuO monoclinic phase. This is understandable because (i) the lattice constants of tetragonal anatase TiO_2 are similar to those of CuO and (ii) the peaks are too broad due to the small crystal size (Nguyen *et al.,* 2013).

The diffraction peaks belonging to monoclinic CuO was observed for the CuO/TiO_2 (1:1) and CuO/TiO_2 (3:1) nanocomposite photocatalyst samples due higher concentration of CuO was used in these samples. While only one peak assigned to anatase TiO_2 was observed in these samples at 2θ of 25.33˚ that could be indexed to (101) plane of anatase TiO_2 and two peak assigned to monoclinic CuO were at 35.48˚ and 38.73˚ could be indexed to (002) and (111) plane, respectively. Demonstrating that TiO_2 and CuO coexist in the CuO/TiO_2 heterojunction (Tayeb & Hussein, 2015). This is reasonable given that the anatase TiO_2 lattice constants are identical to those of CuO. The intensity of the peaks of CuO and TiO_2 decreased in the CuO/TiO_2 bimetallic. It is interesting to note that the visibility of CuO peaks (plane 002 and 111) was more visible in the (1:1) and (3:1) CuO/TiO_2 than the (0.25:1) and (0.5:1) CuO/TiO_2 and the TiO_2 peaks plane 101 was more intense in the CuO/TiO_2 nanocomposite samples of (0.25:1) and (0.5:1). This showed the difference in the composition of the two metal oxides (Bopape *et al.,* 2023).

Interestingly, the peaks assigned to rutile TiO_2 phase was observed for the CuO/TiO_2 nanocomposite samples of (5:1) and (8:1) weight ratio. Similar finding was reported previously by Hanaor & Sorrell, 2011 stated that the presence of a combination of anatase and rutile TiO_2 phases

in the sample with high concentration of dopant because the dopant promoted the transformation of anatase into rutile phase. Therefore, at high concentration of CuO loading, rutile TiO_2 can be observed because it's more stable than anatase TiO_2. As shown in Figure 4(e), for CuO/TiO_2 (5:1) nanocomposite photocatalyst sample the rutile TiO_2 phase was formed as a peak appeared at 2θ of 27.40°, 41.18°, 44.01° and 56.57° that could be assigned to (110), (111), (210) and (220) plane of rutile TiO_2 phase. While the peaks at 2θ 48.70° and 54.25° could be indexed to (200) and (105) anatase TiO_2. The peaks at 2θ of 36.01° and 38.74° with indexed number of (002) and (111) exhibited monoclinic CuO. Similar pattern was detected for CuO/TiO_2 (8:1) nanocomposite photocatalyst samples, except the additional of two peaks at 2θ of 68.96° and 69.69° which are corresponding to (002) and (113) monoclinic CuO.

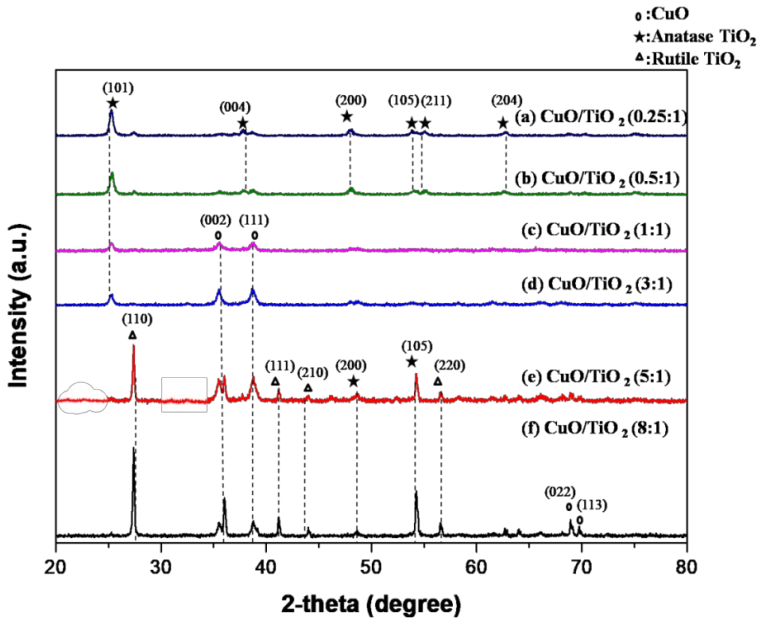

Fig. 4. XRD pattern of CuO/TiO_2 nanocomposite photocatalyst at different ratio.

3.3. BET specific area

To investigate the surface area and porosity of CuO, TiO_2 and CuO/TiO_2 nanocomposite photocatalyst samples, nitrogen gas adsorption-desorption analysis was carried. As tabulate in Table 1, the surface areas of pristine TiO_2 are low which is only 15.26 m^2/g due to the agglomeration of synthesized TiO_2 particles. In contrast, pristine CuO had slightly larger surface area as compared to TiO_2 with 20.50 m^2/g probably due to their smaller particle size. While the surface area of CuO/TiO_2 nanocomposite photocatalyst was found to be 37.12 m^2/g, which is higher than CuO and TiO_2. This may be due to the existence of new pores resulting from the formation of CuO and TiO_2 composites. More surface-active sites may be available with a larger surface area as well as make charge carrier movement easier (Lettieri *et al.,* 2021) and increases surface reabsorption of organic molecules, reducing the recombination of photogenerated electrons and holes (Bensouyad & Bensaha, 2022). Both are beneficial to photocatalytic efficiency performance and the higher surface area of CuO/TiO_2 nanocomposite photocatalyst suggests that this composite may be particularly effective at reducing organic pollutants (Taufik *et al.,* 2018).

Similar results were observed for the pore volume of the samples, with pure CuO and TiO_2 samples having pore volumes of 0.15 cm^3/g and 0.05 cm^3/g, respectively, and the CuO/TiO_2 nanocomposite photocatalyst showing the highest values with 0.20 cm^3/g. While pore size of all studied samples is within 16 to 41 nm suggesting that the samples are mesoporous materials. According to the IUPAC, a mesoporous material is a substance has pored that range in size from 2 to 50 nm. The surface area, pore volume, and pore size of the CuO, TiO_2, and CuO/TiO_2 (1:1) nanocomposite photocatalyst samples are displayed in Table 1.

Table 1. The surface area, pore volume and pore size of CuO, TiO_2 and CuO/TiO_2 nanocomposite photocatalyst.

Sample	Specific surface area (m^2/g)	Pore volume (cm^3/g)	Pore size (nm)
CuO	20.50	0.15	41
TiO_2	15.26	0.05	16
CuO/TiO_2 (1:1)	37.12	0.20	31

According to research in the literature, controlling the large surface area of the photocatalyst, which will contribute to the effectiveness of photocatalytic activity, requires varying the weights of CuO or TiO_2 in nanocomposite photocatalyst ratios (Fadl *et al.,* 2018). Table 2 presented the surface area, pore volume and pore size of the CuO/TiO_2 nanocomposite photocatalyst at different ratio. The surface area of the nanocomposite photocatalyst was slightly increased from 50.85 m^2/g to 51. 99 m^2/g when the weight ratio of CuO was increased from 0.25 to 0.5 over TiO_2. However, at 1:1 ratio of CuO/TiO_2 nanocomposite the surface area is 37.12 m^2/g, which is lower than (0.25;1) and (0.5:1) CuO/TiO_2 samples. This probably due to the agglomeration of nanocomposite photocatalyst. Further increment of CuO into the TiO_2 nanocomposite sample reduced further the surface area into 31.89 m^2/g, 30.04 m^2/g and 26.59 m^2/g because the presence of more CuO contributed to the agglomeration of the nanocomposite samples. Increased copper oxide doping also caused copper oxide clusters to clog pores, reducing the surface are (Richardson *et al.,* 2013). Higher ratio of CuO doping also reduces the pore size and pore volume, as could be seen for CuO/TiO_2 (1:1), CuO/TiO_2 (3:1), CuO/TiO_2 (5:1) and CuO/TiO_2 (8:1) nanocomposite photocatalyst samples in Table 2.

Table 2. The surface area, pore volume and pore size of CuO/TiO_2 nanocomposite photocatalyst at different ratio.

Sample	Specific surface area (m^2/g)	Pore volume (cm^3/g)	Pore size (nm)
CuO/TiO_2 (0.25:1)	50.85	0.46	32
CuO/TiO_2 (0.5:1)	51.99	0.48	35
CuO/TiO_2 (1:1)	37.12	0.20	31
CuO/TiO_2 (3:1)	31.89	0.19	23
CuO/TiO_2 (5:1)	30.04	0.18	22
CuO/TiO_2 (8:1)	26.59	0.13	20

At relative pressures between 0.8 and 1, the CuO, TiO_2, and CuO/TiO_2 (1:1) nanocomposite photocatalyst samples in Figure 5(a), (b) and (c), respectively, show a similar pattern that is type IV with a hysteresis loop, demonstrating the distribution of pores size in the mesoporous area (2 to 50 nm).

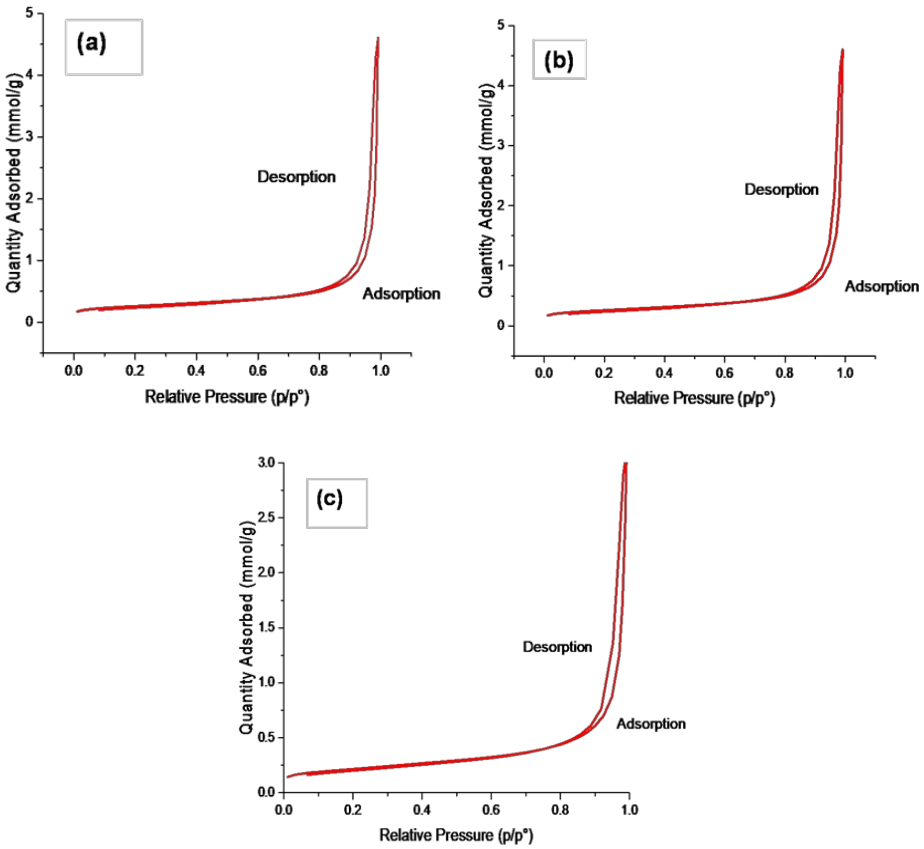

Fig. 5. Isotherms of nitrogen adsorption-desorption photocatalysts a) CuO, b) TiO_2, and c) CuO/TiO_2 (1:1) nanocomposite photocatalyst.

Meanwhile, the H3 type characteristic for the slit-shaped pores matches the hysteresis seen in the isotherms plot (Table 3). Type H_3 hysteresis loops are generally delivered by adsorbents with slit-shaped pores or aggregates of platelet particles (Williams & Reed, 2006). It was connected to the mesoporous capillary condensation, which demonstrates the effective synthesis of the three-dimensional cross-linked structure. The photocatalysts' mesoporous structure helps in the transfer of products and the adsorption of reactants, which increases the photodegradation of pollutants.

Table 3. Types of isotherms, hysteresis, pores and shape of pores CuO, TiO_2 and CuO/TiO_2 (1:1).

Element	Type of isotherms	Type of hysteresis	Type of Pores	Shape of pores
CuO	IV	H3	Mesopore	Slit shaped pores
TiO_2	IV	H3	Mesopore	Slit shaped pores
CuO/TiO_2 (1:1)	IV	H3	Mesopore	Slit shaped pores

Isotherm plot for CuO/TiO_2 nanocomposite photocatalyst at different ratio were shown in Figure 6. Similar plot were observed for all studied sample in this research which is type IV isotherm and type H3 for the hysteresis loop stating that the nanocomposite are in mesopores with slit-shaped pores (Table 4). It can be concluded that the size and shape of pores were not changed with the addition of CuO into TiO_2 to produce nanocomposite photocatalyst.

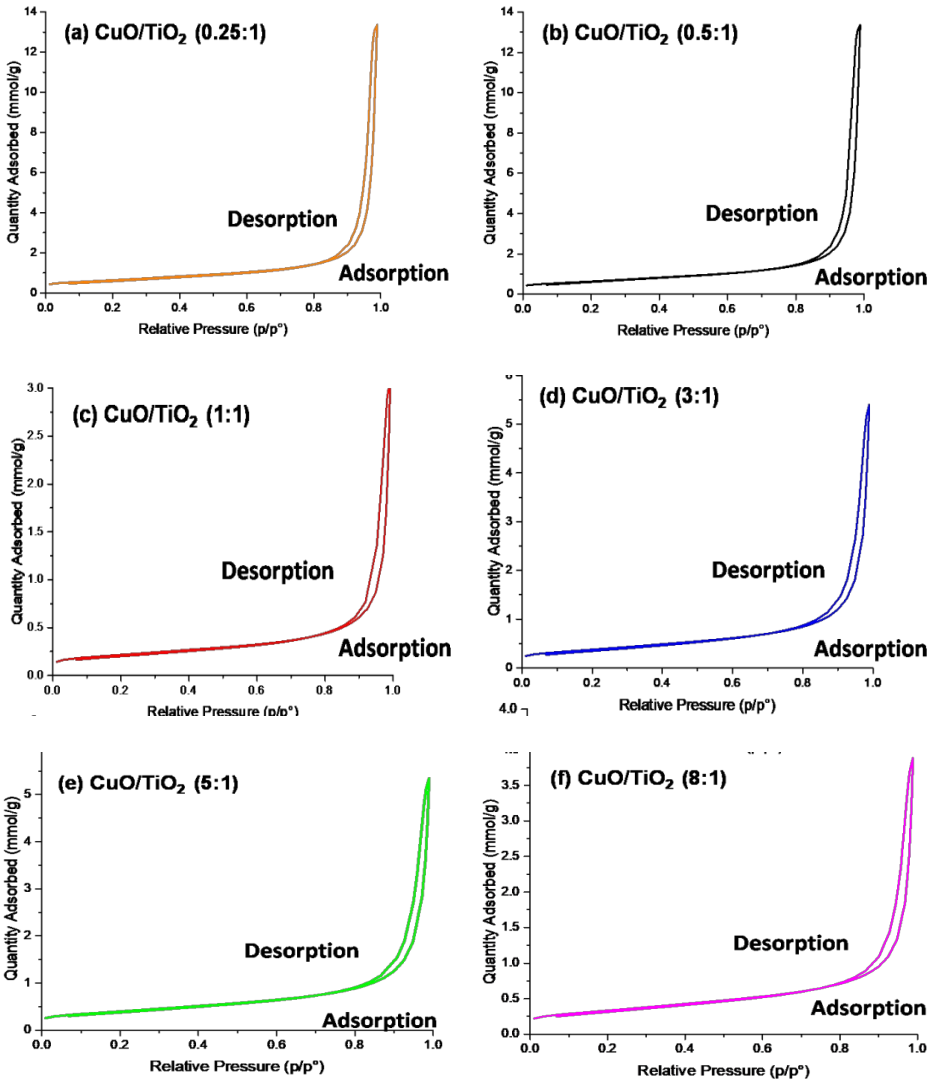

Fig. 6. Isotherms of nitrogen adsorption-desorption photocatalysts (a) 0.25:1, (b) 0.5:1, (c) 1:1, (d) 3:1, (e) 5:1 and (f) 8:1 nanocomposite photocatalyst.

Consistency of type and shape of pores are very important to ensure the efficiency and effectiveness of pure and nanocomposite photocatalyst to degrade pollutants including dyes.

Table 4. Types of isotherms, hysteresis, pores, and shape of pores CuO/TiO_2 with different ratio of CuO.

Element	Type of isotherms	Type of hysteresis	Type of Pores	Shape of pores
CuO/TiO_2(0.25:1)	IV	H3	Mesopore	Slit shaped pores
CuO/TiO_2 (0.5:1)	IV	H3	Mesopore	Slit shaped pores
CuO/TiO_2 (1:1)	IV	H3	Mesopore	Slit shaped pores
CuO/TiO_2 (3:1)	IV	H3	Mesopore	Slit shaped pores
CuO/TiO_2 (5:1)	IV	H3	Mesopore	Slit shaped pores
CuO/TiO_2 (8:1)	IV	H3	Mesopore	Slit shaped pores

3.4. Morphological characterization

Figure 7 displays SEM images of photocatalysts made of CuO, TiO_2, and CuO/TiO_2 nanocomposite materials. The particles of the copper oxide samples, as shown in Figure 7(a), were

probably of an amorphous shape. CuO was measured to have a diameter of 14 nm and a length of 285 nm. Due to some degree of particle agglomeration, the surface of the CuO sample was uneven and rough. Figure 7(b) showed the shape of TiO_2. The TiO_2 particle's form was almost spherical, homogeneous, and agglomerated. The biggest diameter is approximately 100 nm, and the smallest is typically 42 nm. Figure 7(c) depicts the existence of CuO particles with an irregular form and agglomerated TiO_2 with a roughly spherical shape, indicating the successful production of a CuO/TiO_2 nanocomposite. CuO/TiO_2 nanocomposite's particle size was determined to be 92.85 nm.

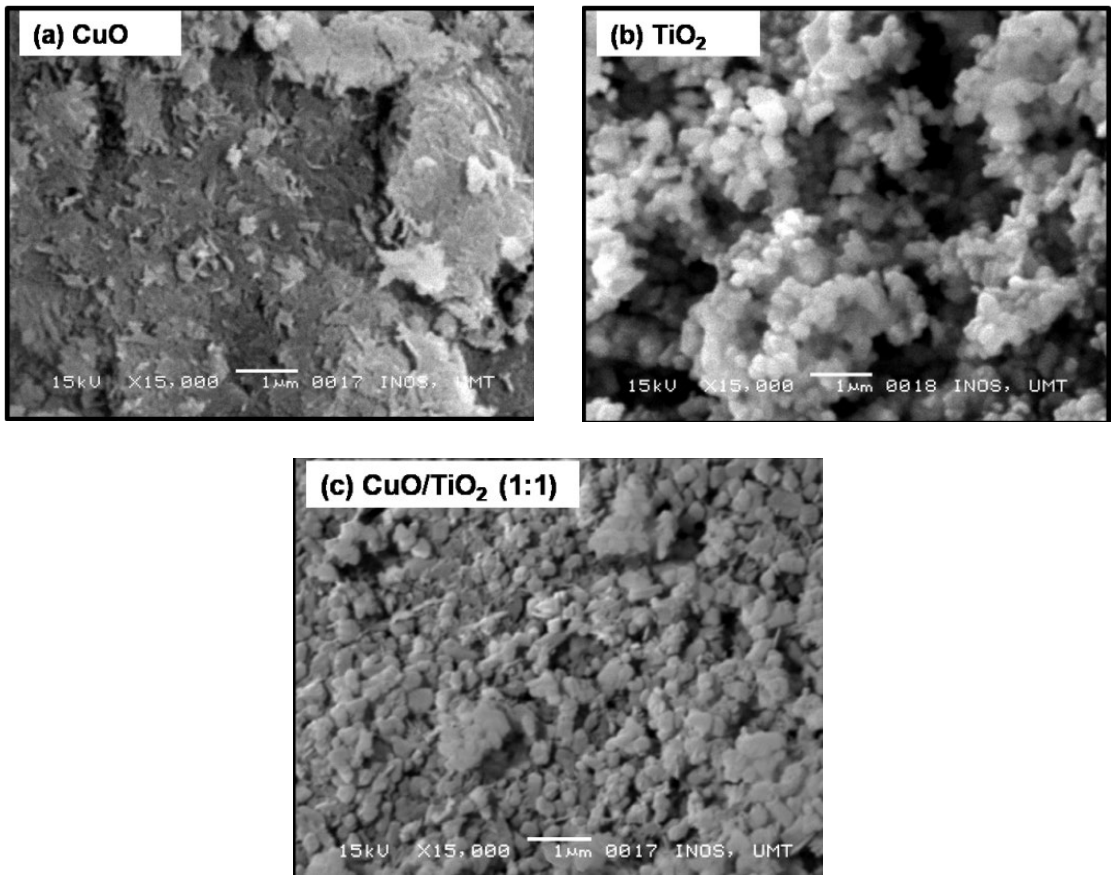

Fig. 7. SEM micrographs of (a) CuO, (b) TiO_2 and (c) CuO/TiO_2 (1:1) nanocomposite photocatalyst with magnification of 15000x.

The SEM images of CuO/TiO_2 nanocomposite photocatalyst sample at different ratio were shown in Figure 8. At low concentration of CuO which are (0.25:1) and (0.5:1) of CuO/TiO_2 samples (Figure 8(a) and (b), the small particles are homogeneously distributed on the surfaces that could be assigned to TiO_2 particle because TiO_2 is the major content of this sample. With the increment of CuO content up to 3 times over TiO_2, the agglomerated nanocomposite particle was observed probably due to interaction of CuO and TiO_2 during calcination process. Similar morphology was obtained by the previous researcher (Mingmongkol *et al.,* 2021). Well spread and homogenously distribution of the particles was indicated in Figure 8(d) and 8(e), because the presence of more CuO in the CuO/TiO_2 (5:1) and (8:1) samples. On top of that, by increasing the amounts of CuO, CuO particles tends to distribute on TiO_2 leading to homogenous surface of CuO/TiO_2 nanocomposite photocatalyst.

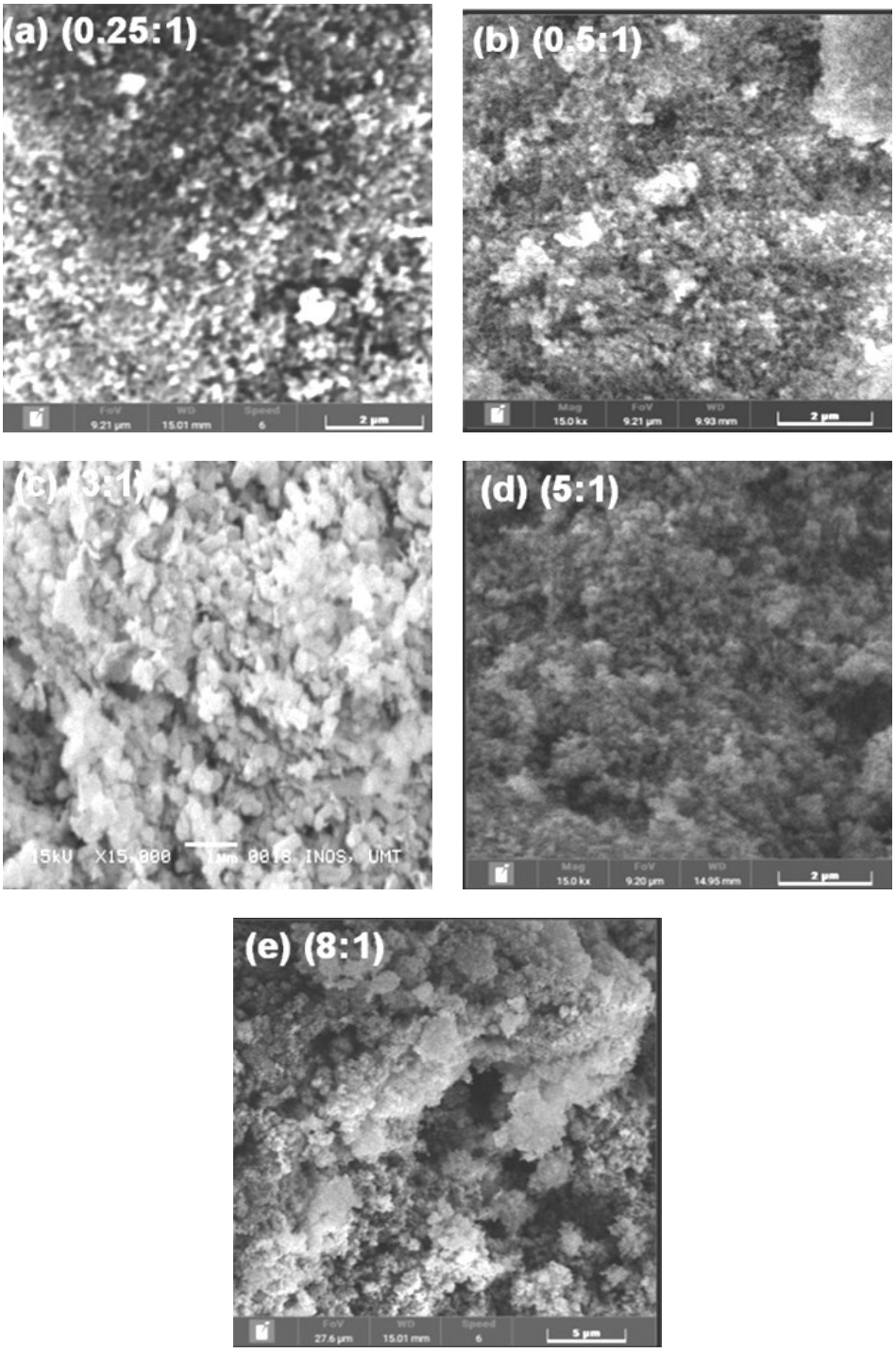

Fig. 8. SEM Image of CuO/TiO_2 (a) 0.25:1, (b) 0.5:1, (c) 3:1, (d) 5:1 and (e) 8:1 nanocomposite photocatalyst with magnification of 15000x.

3.5. Energy dispersive x-ray analysis

The energy dispersive x-ray (EDX) analysis of CuO/TiO_2 nanocomposite photocatalyst was conducted to look into the presence of copper, titanium, and oxygen element in the CuO/TiO_2 nanocomposite photocatalyst and to observe their distribution. The EDX spectra and elemental mapping distribution of CuO/TiO_2 nanocomposite photocatalyst at various ratio was depicted in Figure 9 - 14. The outcomes show that the copper was successfully applied in the TiO_2 sample. The peaks of copper, titanium and oxygen elements appeared at Cu= 0.930 keV, Cu= 8.050 keV, Ti= 0.398 keV, Ti= 4.516 keV and O= 0.528 keV.

The amount of copper presence in the nanocomposite photocatalyst was increased with the increment of copper weight ratio (Table 5). This is because the concentration of Cu species in the nanocomposite sample was increased with the increment of CuO ratio, therefore more copper element was detected in EDX spectra. The Cu, Ti and O element were homogenously distributed in the sample as shown by the elemental mapping analysis. Blue, red, and green colors represent the element of copper, titanium, and oxygen, respectively.

Table 5. Elemental compositions of Cu, Ti, and O (wt %) obtained from EDX in CuO/TiO_2 at different ratio of copper oxide.

Sample	Cu (wt %)	Ti (wt %)	O (wt %)
(a) CuO/TiO_2 (0.25:1)	2.92	50.37	46.71
(b) CuO/TiO_2 (0.5:1)	11.34	66.13	22.53
(c) CuO/TiO_2 (1:1)	32.35	43.57	24.08
(d) CuO/TiO_2 (3:1)	40.7	34.04	25.26
(e) CuO/TiO_2 (5:1)	53.37	21.54	25.09
(f) CuO/TiO_2 (8:1)	55.99	13.82	30.19

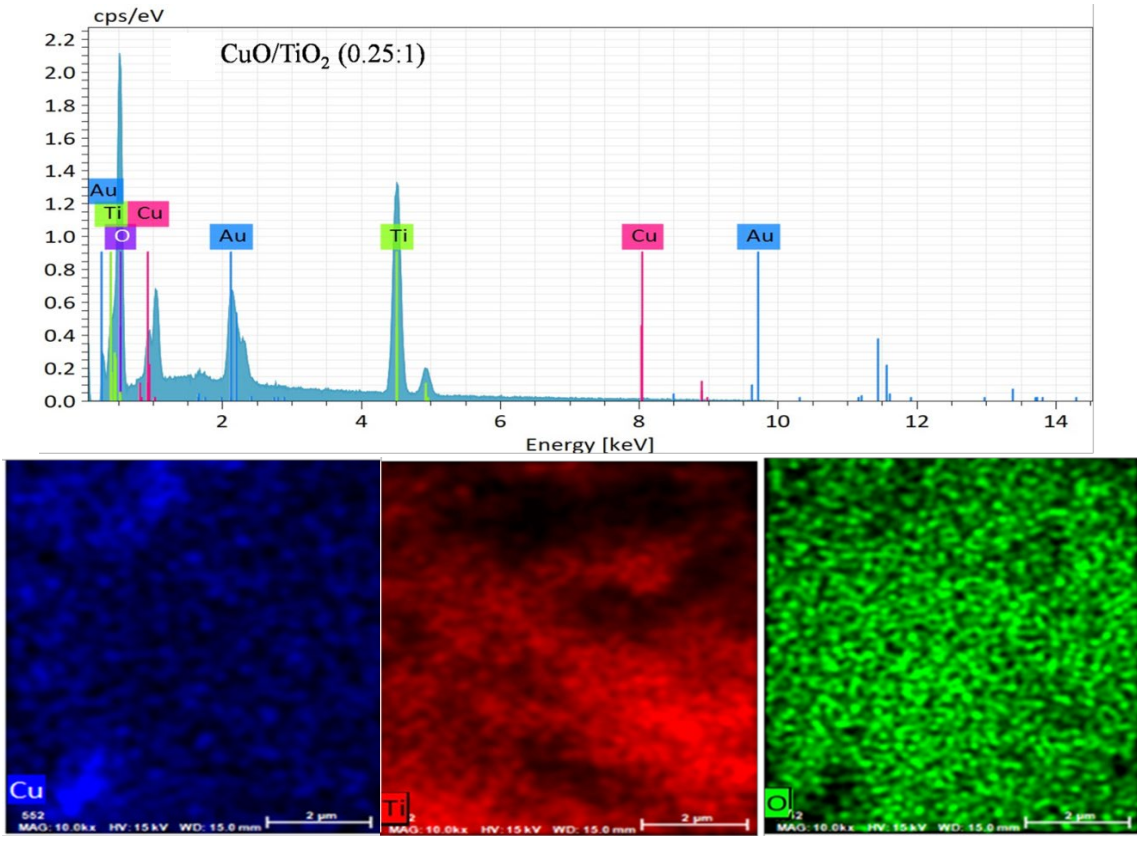

Fig. 9. EDX graph and elemental mapping images of (a) CuO/TiO_2 (0.25:1) photocatalyst.

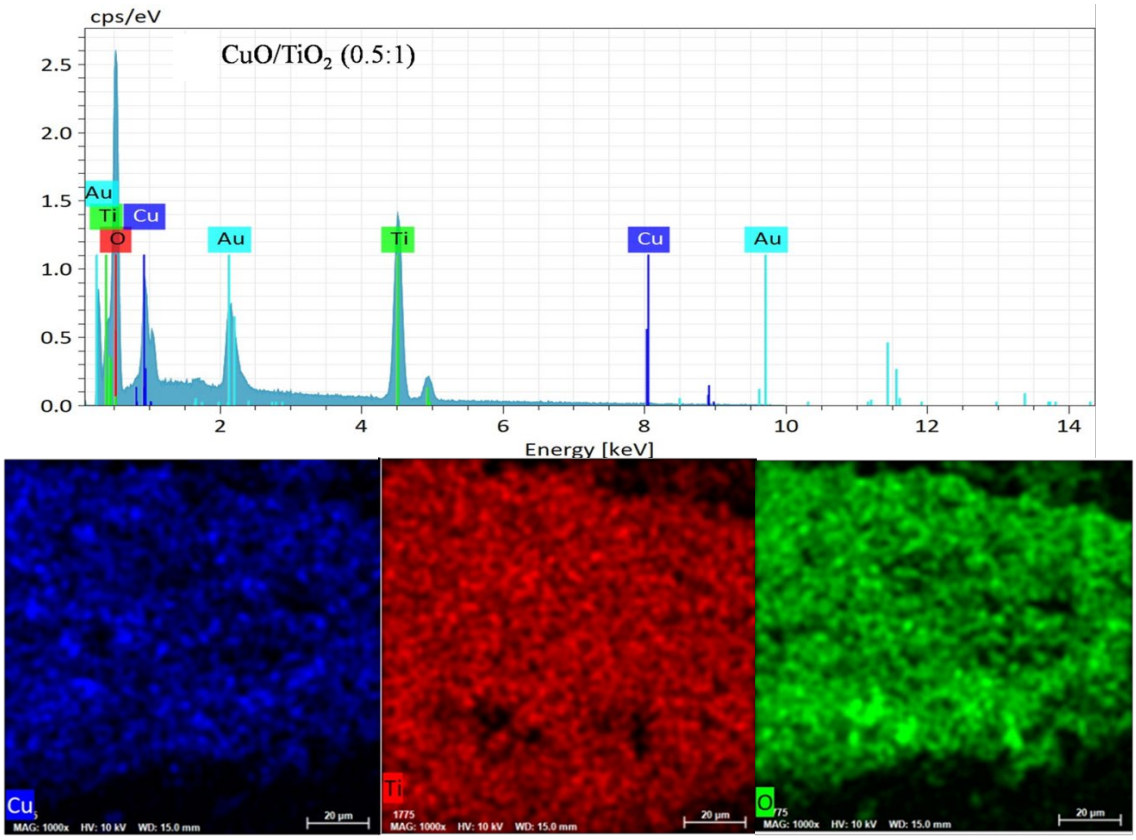

Fig. 10. EDX graph and elemental mapping images of CuO/TiO_2 (0.5:1) photocatalyst.

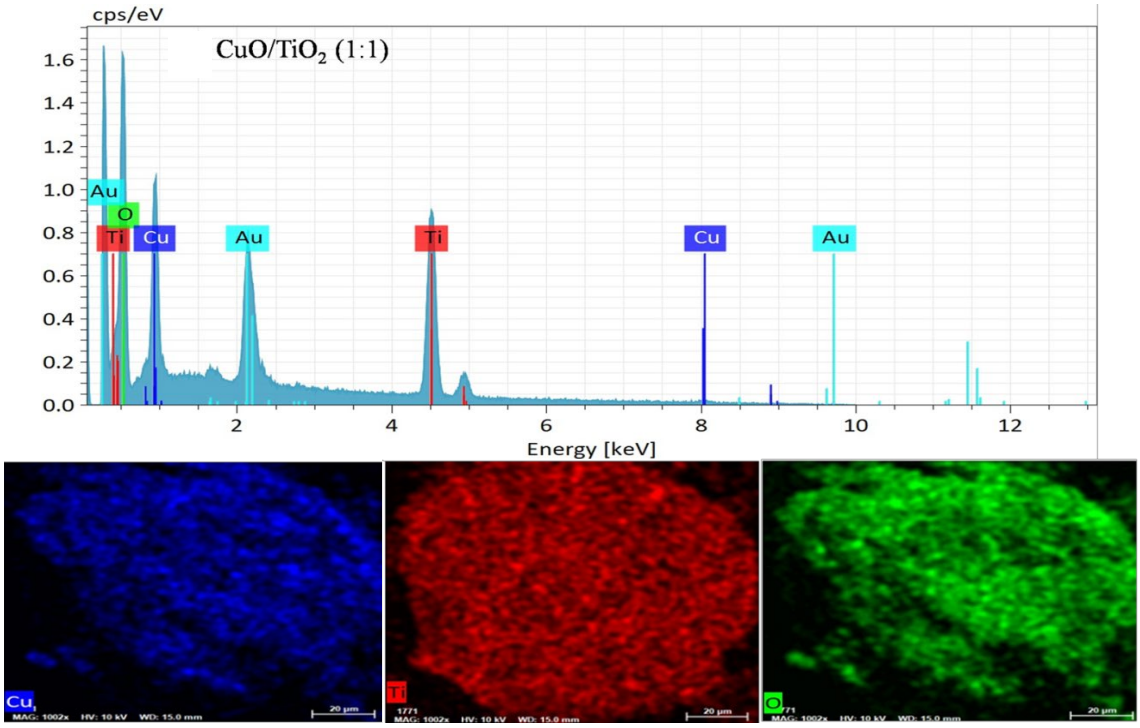

Fig. 11. EDX graph and elemental mapping images of CuO/TiO_2 (1:1) photocatalyst.

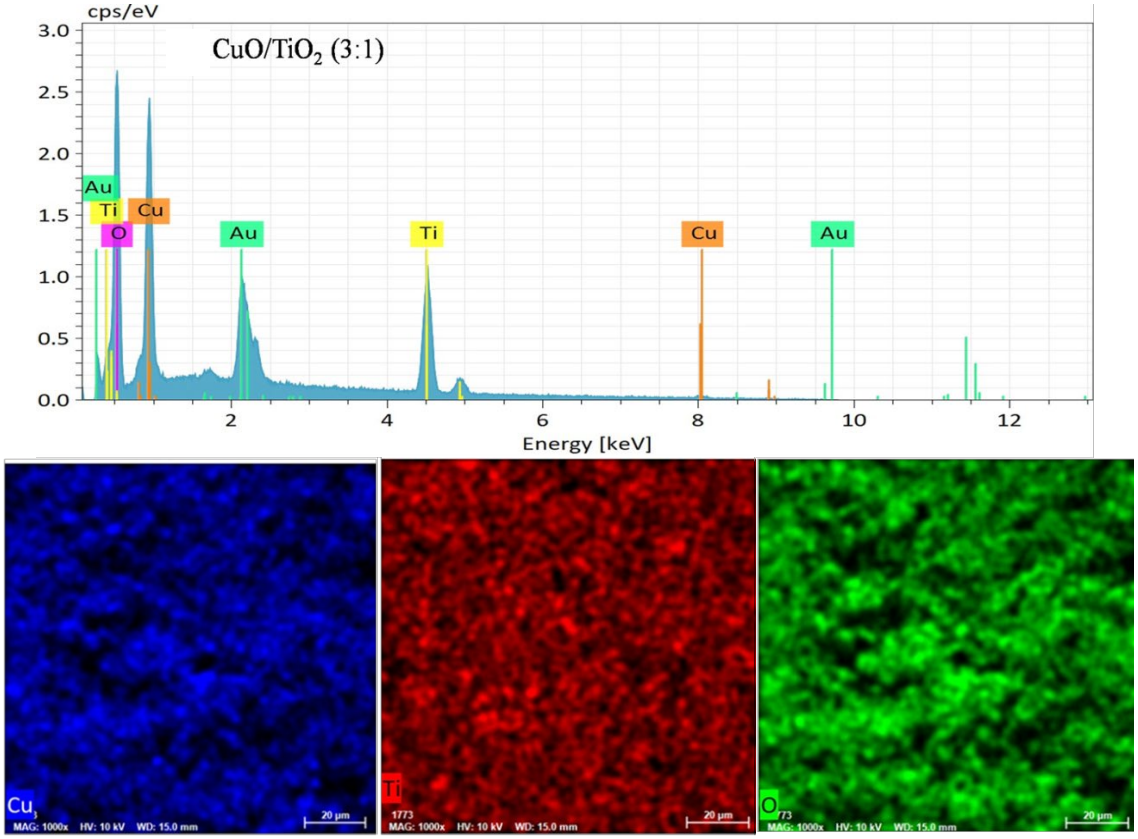

Fig. 12. EDX graph and elemental mapping images of CuO/TiO_2 (3:1) photocatalyst.

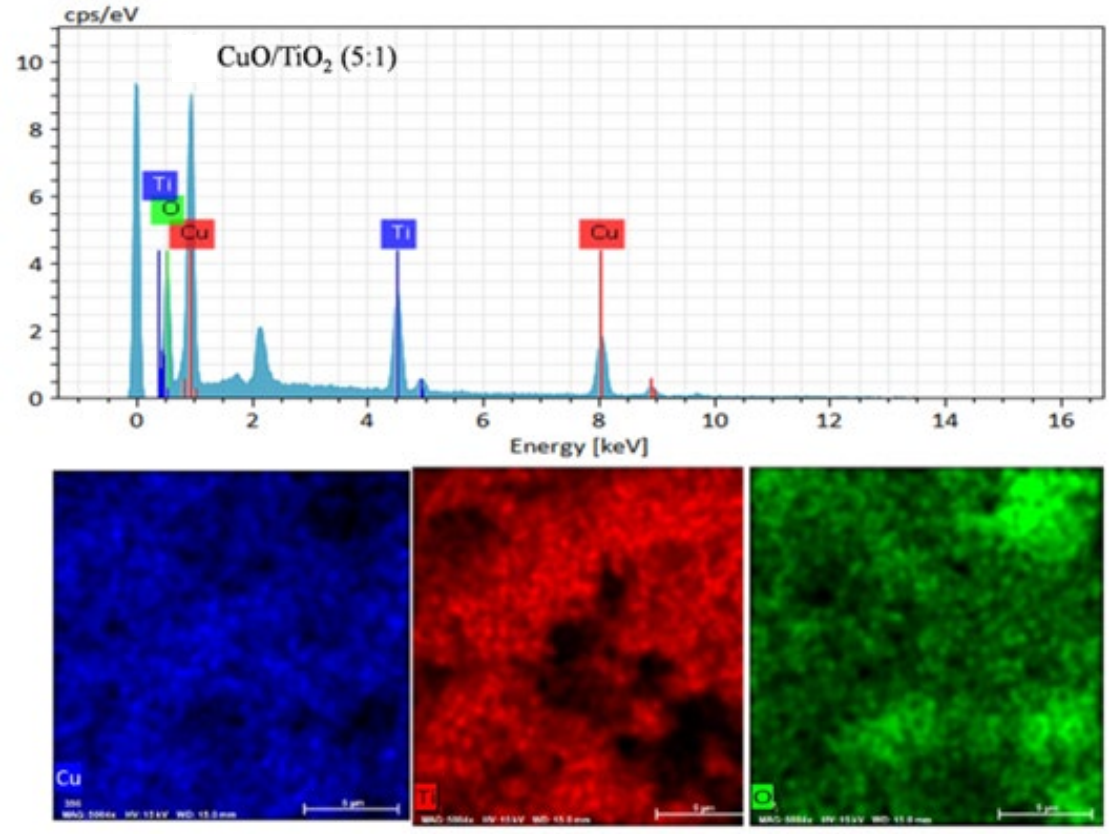

Fig. 13. EDX graph and elemental mapping images of CuO/TiO_2 (5:1) photocatalyst.

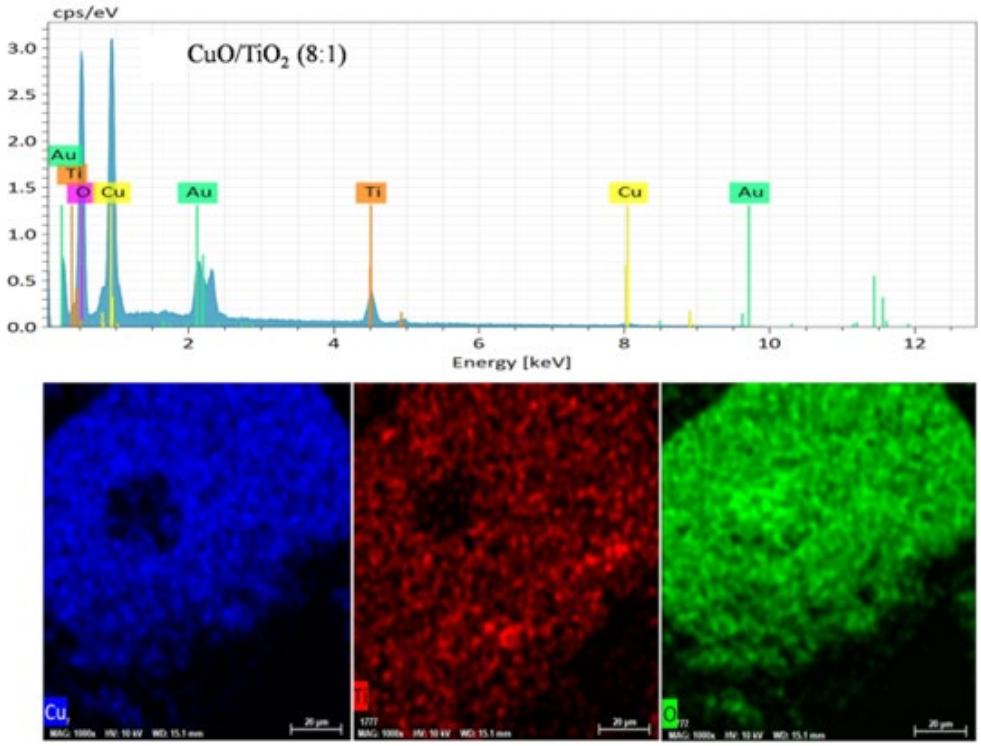

Fig. 14. EDX graph and elemental mapping images of CuO/TiO_2 (8:1) photocatalyst

3.6. Thermal stability

Figure 15 shows the TGA curve for the pure CuO and TiO_2 photocatalyst samples. The total mass loss was found to be 6.7 % and 6.8 % for the CuO and TiO_2 samples, respectively associated with the removal of surface-bound water (Sallem *et al.,* 2017). Water adsorbed on the surface and water produced by condensation of the terminal Cu-OH and Ti–OH molecules to form the CuO and TiO_2 lattice might be causes of lost water. All the analyzed materials exhibited good thermal stability up to 900 °C, which is in line with the literature already available (Tamaekong *et al.,* 2014).

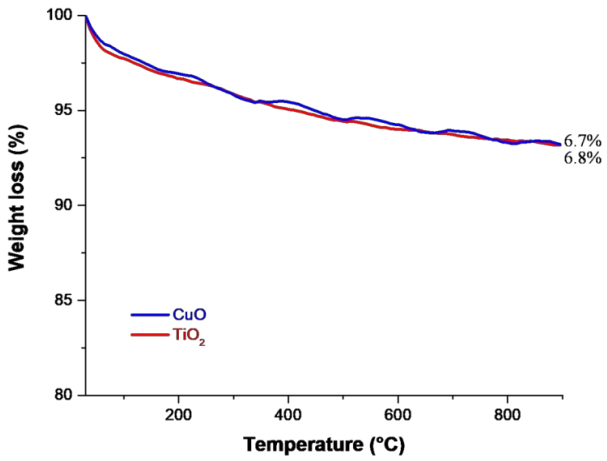

Fig. 15. TGA curves of pure CuO and TiO_2 photocatalyst.

While the TGA curve for CuO/TiO_2 nanocomposite photocatalyst of ratio (0.25:1), (0.5:1), (1:1) and (3:1) were shown in Figure 16, two losses of mass are observed, resulting from the removal of water with the CuO_2 to CuO phase transition. The phase transition from copper (II) oxide to copper (IV) oxide in an inert gas atmosphere (nitrogen) has been described by other researchers, such as Son *et al.,* 2009 and Svintsitskiy *et al.,* 2013. The total mass losses for CuO/TiO_2 nanocomposite at weight ratio of 0.25:1, 0.5:1. 1:1 and 3:1 was 4.4 %, 5.9 %, 7.9 % and 9.4 %, respectively. This data shows that the CuO/TiO_2 nanocomposite photocatalyst is stable to temperature because the mass loss is less than 10 % for all the samples that have been studied in this research. However, the increment in the content of copper oxide reduces the thermal stability of the nanocomposite sample because more $CuSO_4.5H_2O$ was used as precursor.

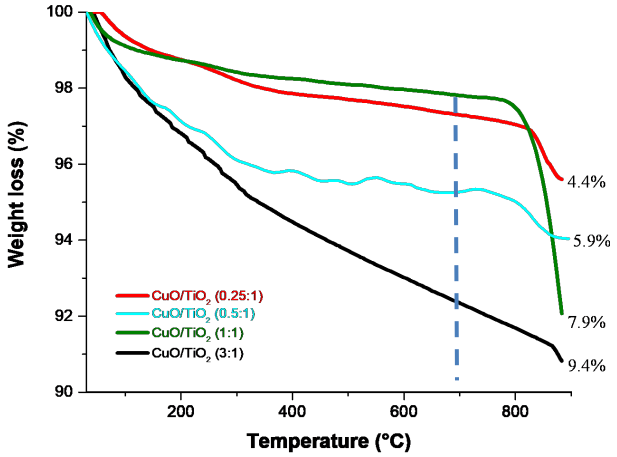

Fig. 16. TGA curves for ratio (0.25:1), (0.5:1), (1:1) and (3:1) of CuO/TiO_2 nanocomposite photocatalyst.

TGA analysis was investigated further on the sample of CuO/TiO_2 nanocomposite photocatalyst with the weight ratio of (5:1) and (8:1). High amount of CuO could affected the thermal stability and decomposition of nanocomposite sample. The TGA curves for each sample are indicated in Figure 17. The sample's overall mass loss was 15.2 % and 23.4 %, respectively. Both samples exhibit a 1-5 % mass loss below 190 °C at greater CuO loading concentrations due to the thermal desorption of surface chemisorbed water. Thermal degradation of supported $CuSO_4.5H_2O$ to CuO and H_2O took place between 190 and 400 °C. (Yoong *et al.,* 2009; Gombac *et al.,* 2010). Thermal oxidation of copper (II) to copper (III) was the cause of the mass loss from 600 °C to 800 °C (Chadda*et al.,* 1989). In this range, mass losses rose in direct proportion to the sample's $CuSO_4.5H_2O$ content. While in the range of 800-900 °C, there is a small weight loss because Cu (III) oxidised to Cu (IV). In general, it can be concluded all studied samples were thermal stability because the weight loss is small (less than 25%) even though the TGA was carried out up to 900°C, which is in line with the literature already available (Tamaekong *et al.,* 2014). The TGA data also showed that the CuO/TiO_2 photocatalyst preparation at 400 °C for 5 hours was suitable, ensuring complete thermal pyrolysis of the $CuSO_4.5H_2O$ precursor to CuO.

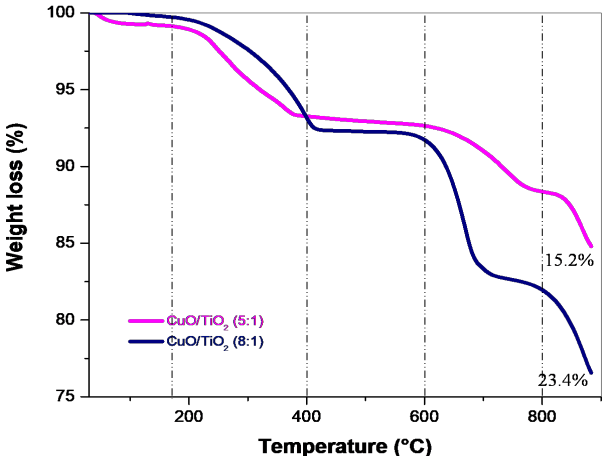

Fig. 17. TGA curves for ratio (5:1) and (8:1) of CuO/TiO_2 nanocomposite photocatalyst.

3.7. Photocatalytic performance

In order to degrade MO under UV light, Figure 18(a) displays the photocatalytic activity of pure CuO, TiO_2, and CuO/TiO_2 (1:1) nanocomposite photocatalyst samples. After 30 minutes, it was discovered that the degradation of MO for nanocomposite photocatalysts made of CuO, TiO_2, and CuO/TiO_2 (1:1) was 5.56 %, 7.81 %, and 9.98 %, respectively. After 3 hours reaction the degradation was increased up to 15.15 %, 25.59 % and 60.00 %. Highest degradation of MO using CuO/TiO_2 (1:1) nanocomposite photocatalyst sample due to the synergistic action from CuO and TiO_2. TiO_2 offers strong charge carrier mobility and produces rapid absorption, while CuO supports further on adsorption of MO onto nanocomposite photocatalyst sample (Moniz & Tang, 2015). While MO degradation using TiO_2 is higher than CuO because of their good photocatalytic properties. It is well known that TiO_2 is a good photocatalytic material since the anatase crystal structure has increased electron mobility. However, because to their small active site and quick electron and hole recombination, pure TiO_2 was only able to degrade MO to a maximum of 25.59 % even after 3 hours process (Xiang *et al.,* 2013). On the other hand, the pristine CuO has reached the maximum absorption capacity level after 3 hours and therefore, the removal of MO cannot reach 100 % removal. Therefore, the combination of TiO_2 with other metal oxide to form the nanocomposite could have improved photocatalytic activity. When compared to pure CuO and TiO_2, the CuO/TiO_2 (1:1) nanocomposite photocatalyst sample in this study demonstrated a greater rate of MO degradation, with 60 % after 3 hours of reaction. Figure 18(b) displays the UV-Vis spectra of MO degradation employing a nanocomposite photocatalyst made of CuO/TiO_2 (1:1).

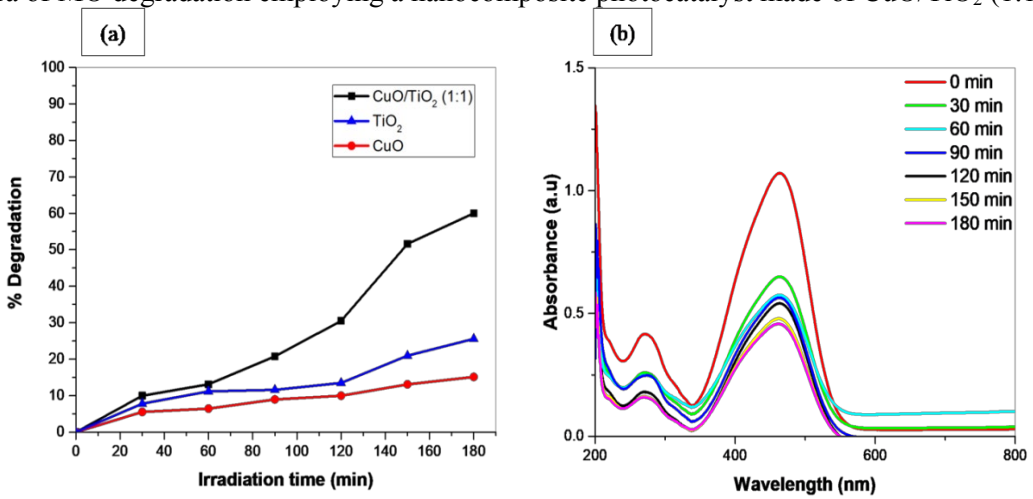

Fig. 18. (a) Degradation of MO using CuO, TiO_2 and CuO/TiO_2 (1:1) nanocomposite photocatayst and (b) UV-Vis spectra of MO degradation using CuO/TiO_2 (1:1) nanocomposite photocatayst.

3.7.1 Photocatalytic activity of copper oxide/titanium dioxide (CuO/TiO_2) nanocomposite photocatalyst

Photocatalytic activity of CuO/TiO_2 nanocomposite photocatalyst at different ratio of CuO was studied. Figure 15(a) demonstrates that after three hours, the CuO/TiO_2 (0.5:1) nanocomposite photocatalyst sample provided the maximum MO degradation with 80.00 % followed by CuO/TiO_2 sample of (0.25:1), (1:1), (3:1), (5:1) and (8:1). Their degradation were 75.00 %, 60.00 %, 19.74 %, 11.71 % and 9.02 % respectively.

The CuO/TiO_2 (0.5:1) nanocomposite sample managed to degrade 80.00 % of MO after 3 hours reaction. This is probably due to their huge surface area and good adsorption of MO using this nanocomposite photocatalyst. In addition, the optimum CuO amounts increase the charge transfer resistance that plays an essential function in preventing photogenerated electrons-holes from recombining (Bharathi *et al.,* 2019). On the other hand, CuO/TiO_2 (8:1) nanocomposite photocatalyst sample shows the lowest photocatalytic activity with only 9.02 % diminishment of MO after 180 minutes due to the high concentration of CuO in nanocomposite photocatalyst sample. The amount of CuO could affects the MO degradation as it involves the adsorption of MO against CuO. However, the presence of CuO at high concentration in nanocomposite photocatalyst sample could clog the adsorption pores, reduce the charge transfer resistance, block the collision of light with photocatalyst and cover the active sites of TiO_2 catalyst that cause inefficiency of photocatalytic process (Singh *et al.,* 2016). Thus, as obtained in this research, the highest ratio of CuO/TiO_2 (8:1) nanocomposite photocatalyst sample recorded the lowest MO degradation rate.

For the sample with less CuO amount such as CuO/TiO_2 (0.25:1) and CuO/TiO_2 (0.5:1) nanocomposite photocatalyst samples, 75.00 % and 80.00 % degradation of MO after 180 minutes were achieved for each sample. The sample with higher CuO ratio over TiO_2 such as (5:1), (3:1) and (1:1), degrade with 11.71 %, 19.74 %, 60.00 %, MO degradation were obtained after 3 hours reaction. Therefore, in this study, it can conclude that the CuO/TiO_2 (0.5:1) nanocomposite photocatalyst was the best photocatalyst with the optimum combination of CuO with TiO_2 since highest degradation of MO (80.00 %) was achieved within 3 hours reaction. Figure 19(b) displays the UV-vis spectra of the degradation of methyl orange in 3 hours reaction using a nanocomposite CuO/TiO_2 (0.5:1) photocatalyst. The maximum absorbance peak of MO at 464 nm was decreased when the reaction time was increased from 30 minutes until 180 minutes because the MO was successfully degraded using CuO/TiO_2 (0.5:1) nanocomposite photocatalyst.

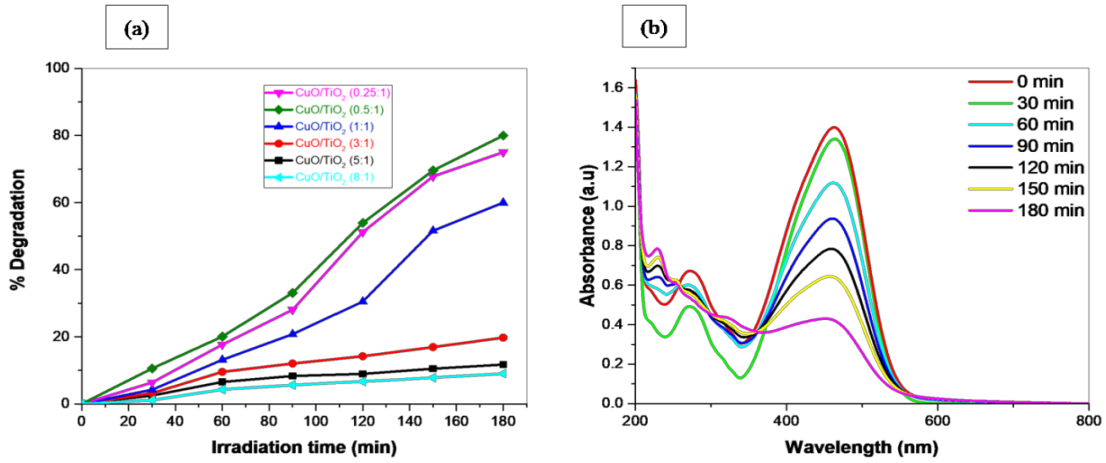

Fig. 19. (a) Degradation of CuO/TiO_2 nanocomposite photocatayst at different ratio and (b) UV-Vis spectra of MO degradation using CuO/TiO_2 (0.5:1) nanocomposite photocatayst.

4. Conclusions

In summary, CuO/TiO_2 nanocomposite photocatalyst was successfully synthesized and characterized using various techniques such as FTIR, XRD, BET, SEM, EDX and TGA. The presence of CuO in CuO/TiO_2 (0.5:1) nanocomposite photocatalyst enhanced the degradation of MO up to 80.00 % compared to pure TiO_2 and CuO for 3 hours reaction, because it acted as photon provider into TiO_2 for better and longer reaction. Moreover, the largest surface area of CuO/TiO_2 (0.5:1) nanocomposite photocatalyst increased the surface area for MO degradation. FTIR result shows the existence of OH stretching, OH bending and metal oxide between TiO_2 with the CuO. XRD peaks was decreased with the increment of CuO concentration attributed the interaction between TiO_2 and CuO. CuO/TiO_2 nanocomposite photocatalyst is more thermally stable as compared CuO and TiO_2. As concluded, 0.1g of CuO/TiO_2 (0.5:1) shows the best photodegradation rate of 20 ppm MO (80.00%).

Acknowledgements

The authors are grateful to Universiti Malaysia Terengganu (UMT) for providing the facilities to carry out this project and Malaysia Ministry of Higher Education for the financial support (FRGS 59571/1/2019/STG07/UMT/02/2).

References

[1] Y.L. Pang, A.Z. Abdullah, Clean-Soil, Air, Water 41 (8), 751-764 (2013); https://doi.org/10.1002/clen.201000318
[2] A.E. Al Prol, Asian Fisheries Science, 3 (2),1-18 (2019); https://doi.org/10.9734/ajfar/2019/v3i230032
[3] M. Ijaz, M. Zafar, International Journal Of Energy Research 45 (3), 3569-3589 (2021); https://doi.org/10.1002/er.6079
[4] X. Kang, S. Liu, Z. Dai, Y. He, X. Song, Z. Tan, Catalysts 9 (2),191 (2019); https://doi.org/10.3390/catal9020191
[5] B. Pant, M. Park, S.J. Park, Coatings 9 (10), 613 (2019); https://doi.org/10.3390/coatings9100613
[6] W.J. Chen, K.C. Hsu, T.H. Fang, C.L. Lee, T.H. Chen, T. H. Hsieh, Digest Journal of Nanomaterial and Biostructures 16, 1227 (2021).
[7] M. Zhu, Y. Mi, G. Zhu, D. Li, Y. Wang, Y. Weng, Journal of Physical Chemistry C 117, 18863-18869 (2013); https://doi.org/10.1021/jp405968f
[8] H. Wang, L. Zhang, Z. Chen, J. Hu, S. Li, Z. Wang, J. Liu, X. Wang, Chemical Society Reviews 43 (15), 5234-5244 (2014); https://doi.org/10.1039/C4CS00126E
[9] W. Kim, T. Tachikawa, H. Kim, N. Lakshminarasimhan, P. Murugan, H. Park, T. Majima, W. Choi, Applied Catalysis A 147, 642-650 (2014); https://doi.org/10.1016/j.apcatb.2013.09.034
[10] A.S. Weber, A.M. Grady, R.T. Koodali, Catalysis Science & Technology 2, 683-693 (2012); https://doi.org/10.1039/c2cy00552b
[11] S.B. Patil, P.S. Basavarajappa, N. Ganganagappa, M.S. Jyothi, A.V. Raghu, K.R. Reddy, International Journal of Hydrogen Energy 44 (26), 13022-13039 (2019); https://doi.org/10.1016/j.ijhydene.2019.03.164
[12] T.M. Khedr, S.M. El-Sheikh, A. Hakki, A.A. Ismail, W.A. Badawy, D.W. Bahnemann, Photochemistry and Photobiology A: Chemistry 346, 530-540 (2017); https://doi.org/10.1016/j.jphotochem.2017.07.004
[13] M. Kudhier, R. Sabry, Y. Al-Haidarie, M. Al-Marjani, Materials Technology 33 (3), 220-226 (2018); https://doi.org/10.1080/10667857.2017.1396778
[14] P. Bezerra, R.P. Cavalcante, A. Garcia, H. Wender, M.A. Martines, G.A. Casagrande, J. Giménez, P. Marco, S.C. Oliveira, A. Machulek, Journal of the Brazilian Chemical Society 28, 1788-1802 (2017).

[15] J.Q. Li, D.F. Wang, Z.Y. Guo, Z.F. Zhu, Applied Surface Science 263, 382-388 (2012); https://doi.org/10.1016/j.apsusc.2012.09.066
[16] M. Wei, J. Wan, Z. Hu, Z. Peng, B. Wang, H. Wang, Applied Surface Science 391, 267-274 (2017); https://doi.org/10.1016/j.apsusc.2016.05.161
[17] A.A. Murashkina, A.V. Rudakova, V.K. Ryabchuk, K.V. Nikitin, R.V. Mikhailov, A.V. Emeline, D.W. Bahnemann, The Journal of Physical Chemistry C 122 (14), 7975-7981 (2018); https://doi.org/10.1021/acs.jpcc.7b12840
[18] S. Liu, G. Liu, Q. Feng, Journal of Porous Materials 17 (2), 197-206 (2010); https://doi.org/10.1007/s10934-009-9281-8
[19] X. Gao, B. Zhou, R. Yuan, Environmental Engineering Research 20 (4), 329-335. (2015); https://doi.org/10.4491/eer.2015.062
[20] S. Phromma, T. Wutikhun, P. Kasamechonchung, T. Eksangsri, C. Sapcharoenkun, Applied Sciences 10 (3), 993 (2020); https://doi.org/10.3390/app10030993
[21] R. Jothiramalingama, T. Radhika, P.R. Aswini, H. Al-Lohedan, M. Chandrasekaran, D.M. Al-Dhayan, J.N. Appaturi. Digest Journal of Nanomaterials & Biostructures 17(2), 491-497 (2022); https://doi.org/10.15251/DJNB.2022.172.491
[22] B. Niu, X. Wang, K. Wu, X. He, R. Zhang, Materials 11 (10), 1910 (2018); https://doi.org/10.3390/ma11101910
[23] N. Cotolan, M. Rak, M. Bele, A. Cör, L.M. Muresan, I. Milošev, Surface and Coatings Technology 307, 790-799 (2016); https://doi.org/10.1016/j.surfcoat.2016.09.082
[24] Y. Kondo, H. Yoshikawa, K. Awaga, M. Murayama, T. Mori, K. Sunada, S. Bandow, S. Iijima, Langmuir 24, 547-550 (2008); https://doi.org/10.1021/la702157r
[25] J. Zhu, F. Chen, J. Zhang, H. Chen, M. Anpo, Journal of Photochemistry and Photobiology A: Chemistry 180 (1-2), 196-204 (2006); https://doi.org/10.1016/j.jphotochem.2005.10.017
[26] R.C. Zulkifli, M.H. Razali, F. Azaman, A. Ali, M.A.A.M. Nor, Materials Science and Engineering 440 (1), 012019 (2018); https://doi.org/10.1088/1757-899X/440/1/012019
[27] X.Q. Cheng, C.Y. Ma, X.Y. Yi, F. Yuan, Y. Xie, J.M. Hu, B.C. Hu, Q.Y. Zhang, Thin Solid Films 615, 13-18 (2016); https://doi.org/10.1016/j.tsf.2016.06.049
[28] Y. Zhang, X. Xu, ACS Omega 5, (25), 15344-15352 (2020); https://doi.org/10.1021/acsomega.0c01438
[29] H. Feng, M.H. Zhang, E.Y. Liya, Applied Catalysis A: General 413, 238-244 (2012); https://doi.org/10.1016/j.apcata.2011.11.014
[30] M.H. Mamat, N. Parimon, A.S. Ismail, I.B.S. Banu, S.S. Basha, R.A. Rani, A.S. Zoolfakar, M.F. Malek, A.B. Suriani, M.K. Ahmad, Materials Research Bulletin 127, 110860 (2020); https://doi.org/10.1016/j.materresbull.2020.110860
[31] D. Li, H. Song, X. Meng, T. Shen, J. Sun, W. Han, X. Wang, Nanomaterials 10 (3), 546 (2020); https://doi.org/10.3390/nano10030546
[32] A.A. Issa, T.A. Hamoudi, Tikrit Journal of Pure Science 27 (3),15-18 (2022) https://doi.org/10.25130/tjps.v27i3.55
[33] Y.J.Choi, Z.Seeley, A. Bandyopadhyay, S. Bose, and S.A. Akbar, 124 (1), 2007. Sensors and Actuators B: Chemical, 111-117 (2007); https://doi.org/10.1016/j.snb.2006.12.005
[34] S. Ghasemi, S. Rahimnejad, S.R. Setayesh, S. Rohani, M.R. Gholami, Journal of Hazardous Materials, 172 (2-3), 1573-1578 (2009); https://doi.org/10.1016/j.jhazmat.2009.08.029
[35] L.G. Devi, B.N. Murthy, S.G. Kumar, Materials Science and Engineering: B, 166 (1), 1-6. (2010); https://doi.org/10.1016/j.mseb.2009.09.008